Letter

Laminar separation bubble bursting in a surging stream

David Greenblatt ⬤[*] and Hanns Müller-Vahl

Faculty of Mechanical Engineering, Technion - Israel Institute of Technology, 3200003 Haifa, Israel

Christoph Strangfeld ⬤

Department of Non-Destructive Testing, Bundesanstalt für Materialforschung und -prüfung,
Unter den Eichen 87, 12205 Berlin, Germany
and Hermann-Föttinger-Institut, Technische Universität Berlin, 10623 Berlin, Germany

The effect of high-amplitude harmonic surging on airfoil laminar separation bubbles, at small angles of attack, was investigated experimentally in a dedicated surging-flow wind tunnel. A generalized pressure coefficient was developed that accounts for local static pressure variations due to surging. This critical generalization facilitated direct comparisons between surging and quasisteady pressure coefficients, and thus unsteady effects could be distinguished from Reynolds number effects. A momentum-integral boundary layer analysis was implemented to determine movement of the bubble separation point, and movement of the transition point was extracted from experimental surface pressure coefficients. The most significant finding was that bubble bursting occurs, counterintuitively, during early imposition of the favorable temporal pressure gradient, because the favorable pressure gradient rapidly drives the bubble aft, rendering it unable to reattach. This surge-induced dynamic stall mechanism resulted in large lift and form-drag coefficient oscillations. Furthermore, failure to implement the generalized pressure coefficient definition resulted in temporal form-drag coefficient errors of up to 400 counts.

I. INTRODUCTION

The effect of periodic longitudinal flow oscillations, or surging, on airfoil boundary layers has been studied for many years [1,2]. These studies are motivated by the need to understand the unsteady aerodynamics of, *inter alia*, rotary wing aircraft in forward flight [3], vertical axis wind turbine operation [4,5], and horizontal axis wind turbines operating in yawed flows [6]. Most of these studies focus on airfoils at high angles of attack, where stall is present [4,5,7–10]. The current investigation considers nominally attached flows, at small angles of attack, with surprising results that offer insights into laminar separation bubble bursting.

The simultaneous generation of large-amplitude surging oscillations relative to the mean velocity ($\sigma \equiv \Delta U / \bar{U}$) at typical flight or turbine Reynolds numbers ($\overline{\text{Re}} \equiv \bar{U} c / \nu$) poses significant technical challenges. This is because either the flow or the test article must undergo large-amplitude oscillations. Recently, two independent relatively high $\{\overline{\text{Re}}, \sigma\}$ experiments [3,11] were performed on NACA 0018 airfoils with nominally attached boundary layers, under the conditions $\{3 \times 10^5, 0.5\}$ and $\{1.5 \times 10^6, 0.2\}$, respectively. In the former investigation, at dimensionless surging frequencies of $k_{\text{su}} \equiv \omega c / 2\bar{U} = 0.1$, comparisons of the lift coefficient as a function of phase angle, $C_l(\phi)$, to classical thin airfoil theory [12–14] were contradictory. With a nominally tripped boundary

---

*davidg@technion.ac.il

layer, the lift coefficient corresponded qualitatively with theory, but high-frequency oscillations were observed following deceleration of the stream. However, without tripping, the lift coefficient amplitude was *opposite* to that of theory, producing an anticorrelation, which was also accompanied by high-frequency oscillations. Reference [11] attempted an explanation based upon a vortex sheet strength comparison, but that operation masked the effect of surging on the separation bubbles. Significant deviations from theory were also observed in the latter investigation [3], particularly at the highest frequency tested, namely $k_{su} = 0.05$. It was suggested that this was due to an interaction of the net induced velocity, arising from the shed circulation, with the boundary and trailing-edge shear layers. However, the authors did not directly investigate unsteady effects on the laminar separation bubbles.

Under a nominally steady freestream, laminar separation bubbles are relatively well understood [15–23], but much is unknown about their response to high-amplitude surging, whose frequency is very much lower than the lowest bubble instability frequency. This dearth of knowledge, coupled with significant deviations from, and anticorrelations with, theory served as the motivation to investigate temporal pressure gradient effects on the airfoil laminar separation bubbles. This was achieved by scrutinizing the surface pressure coefficients, where a generalized pressure coefficient was defined in order to correctly interpret temporal pressure gradient effects. This generalization is critical to understanding the separation mechanism as well as accurately computing the integral aerodynamic coefficients. In order to isolate purely unsteady effects from the influence of Reynolds number, pressure coefficients associated with surging were compared with those generated under quasisteady conditions. In addition, a momentum-integral approach was adopted to predict the movement of the bubble separation point. Finally, the theoretical and experimental approaches were combined to reveal the mechanism of bubble bursting in a surging stream.

II. THEORETICAL CONSIDERATIONS

A. Pressure coefficient in a surging stream

For the purpose of our discussion, we define a harmonically surging stream in an incompressible flow as

$$U(t) = \bar{U}(1 + \sigma \sin \omega t), \tag{1}$$

where $\bar{U}$ is the mean freestream velocity. The local freestream static pressure is denoted as $p_{st} = p_{st}(x, t)$. In experiments, p_{st} cannot be unambiguously measured along the tunnel walls because, in general, wall pressures respond to both test section pressure variations and test article load variations. To circumvent this coupling, $p_0(0, t)$ and $U(t)$ are measured simultaneously at $x = 0$ and the stagnation pressure coefficient definition $C_p(0, t) \equiv [p_0(0, t) - p_{st}(0, t)]/q(t) = 1$ is used to obtain

$$p_{st}(0, t) = p_0(0, t) - q(t), \tag{2}$$

where $q(t) = \frac{1}{2}\rho U^2$. Next, Eq. (1) is substituted into Euler's equation,

$$\frac{1}{\rho} \frac{\partial p_{st}}{\partial x} = -\frac{dU}{dt}, \tag{3}$$

and integrated to yield

$$p_{st}(x, t) = p_{st}(0, t) - x\rho \bar{U}\sigma \omega \cos \omega t. \tag{4}$$

Finally, for an arbitrary test article surface pressure $p(x, t)$, the local pressure coefficient is defined as

$$c_p(x, t) \equiv [p(x, t) - p_{st}(x, t)]/q(t), \tag{5}$$

which, after substitution of Eq. (4), results in

$$c_p(x,t) = [p(x,t) - p_{st}(0,t) + x\rho\bar{U}\sigma\omega\cos\omega t]/q(t) \tag{6}$$

or

$$c_p(x,t) = \frac{p(x,t) - p_{st}(0,t)}{q(t)} + C(x,t), \tag{7}$$

where the first term on the right-hand side is the standard, or uncorrected, pressure coefficient c_{pu}, and the correction term,

$$C(x,t) = 4\sigma k_{su}\hat{x}\frac{\cos\omega t}{(1+\sigma\sin\omega t)^2}, \tag{8}$$

with $\hat{x} \equiv x/c$. In contrast to pitching airfoils, where quasisteady effects are assumed for $k_{pi} \equiv \omega c/2\bar{U} < 0.002$ [24], quasisteady surging flows ($c_{pu} \approx c_p$) require that $C(c,t) \ll 1$ for all t. We shall refer to Eq. (6) or Eqs. (7) and (8) as the generalized pressure coefficient.

B. Unsteady integral boundary layer analysis

Consider an airfoil boundary layer subjected to an external boundary condition, or edge velocity $U_e(s,t)$, where the coordinate s is measured from the stagnation point, along the surface of the airfoil. The unsteady momentum integral equation has the form

$$\frac{\tau_w}{\rho} = \frac{\partial(U_e^2\theta)}{\partial s} + \delta^*U_e\frac{\partial U_e}{\partial s} + \frac{\partial(U_e\delta^*)}{\partial t}, \tag{9}$$

which, apart from the time dependence expressed in the last term, is identical to the standard steady form [25]. Equation (9) presents a "closure" problem, because a presently unknown theoretical or empirical expression for $\delta^*(t)$ must be introduced [26]. We circumvent this problem by using the quasisteady version of Eq. (9), i.e., by neglecting the last term. Justification for this is obtained by expanding the last term and comparing its absolute value to the absolute value of the second-to-last term, for the present problem. This allows us the considerable simplification of employing the well-known Pohlhausen velocity profile [25], together with the generalized boundary layer parameter [26],

$$K \equiv \frac{\theta^2}{\nu}\left(\frac{\partial U_e}{\partial s} + \frac{1}{U_e}\frac{\partial U_e}{\partial t}\right), \tag{10}$$

where $K = -0.1567$ indicates the separation point. Thus the flow state, and in particular boundary layer separation point, is determined by a combination of the spatial adverse pressure gradient produced by the airfoil geometry and angle of attack,

$$K_s = \frac{\theta^2}{\nu}\frac{\partial U_e}{\partial s} = \hat{Q}\frac{\partial \hat{U}_e}{\partial \hat{s}}, \tag{11}$$

and the temporal pressure gradient produced by the surging stream,

$$K_t = \frac{\theta^2}{\nu U_e}\frac{\partial U_e}{\partial t} = 2\hat{Q}\sigma k_{su}\frac{\cos\omega t}{(1+\sigma\sin\omega t)^2}, \tag{12}$$

where the dimensionless quadrature term is

$$\hat{Q} = \hat{Q}(\hat{s},t) = \frac{0.47}{\hat{U}_e^6}\int_0^{\hat{s}}\hat{U}_e^5 d\hat{s}. \tag{13}$$

In Eqs. (11) and (13) above, $\hat{s} \equiv s/c$ and $\hat{U}_e \equiv U_e/\bar{U}$. To compute the time-dependent separation point, we use a vortex-lattice method [27] to obtain $\hat{U}_e$ and $\partial\hat{U}_e/\partial\hat{s}$, for a given α. The former facilitates the quadrature calculation of Eq. (13), and hence K_s and K_t are computed. The expression

$K_s + K_t = -0.1567$ is then solved numerically as a function of the phase angle $\phi \equiv \omega t$ to obtain $\hat{s}_{\mathrm{sep}}$ and hence $\hat{x}_{\mathrm{sep}}$. Note that the *quasisteady flow conditions*, corresponding to $K_t = 0$ and referred to in Sec. II A, are different from the *quasisteady boundary layer assumptions* invoked in this section.

III. EXPERIMENTAL SETUP AND METHODS

Experiments were carried out in a blow-down wind tunnel, that incorporates a $1004 \times 610 \times 4070$ mm test section [28], a top speed of 55 m/s, and a turbulence level of less than 0.1%. A louver system, mounted at the test section exit and driven by a servomotor, was used to vary the exit area and hence the freestream velocity. A NACA 0018 airfoil (chord $c = 348$ mm and span of $b = 610$ mm) was mounted 0.91 m downstream of the test section nozzle. It was equipped with a 1.2-mm-wide passive slot at 5% chord, which acted as a boundary layer trip. The tripped (slotted) side of the airfoil was defined as the upper surface, i.e., the low-pressure surface for $\alpha > 0°$, and the smooth side as the lower surface. Forty-four symmetrically disposed pressure ports were close coupled to piezoceramic pressure transducers inside the model. Six additional pressure ports were located at chordwise positions of $\hat{x} = 21.5\%$ and 69.5% on the suction surface as well as $\hat{x} = 69.5\%$ on the pressure surface at a distance of 100 mm from each side wall. Surface pressures were continuously recorded at a sample rate of 499 Hz and subsequently phase averaged. Simultaneously, the instantaneous averages of two hot-wire measurements ahead of the airfoil (above and below), were phase-averaged to determine $U(t)$. Harmonic surging and quasisteady data were acquired between $\alpha = -4°$ and $4°$ in steps of $1°$ and at $8°$, under the conditions $k_{\mathrm{su}} = 0.1$, $\mathrm{Re} = 3 \times 10^5$, and $\sigma = 0.5$. The physical surging frequency, namely 1.2 Hz, was at least two orders of magnitude lower than the lowest anticipated bubble instability frequency [29]. Full details of the experimental setup are provided in Ref. [11].

IV. RESULTS AND DISCUSSION

A. Airfoil pressure distributions

The results presented in this section rely on a direct comparison between unsteady and quasisteady pressure coefficient distributions at identical Reynolds numbers, in order to quantify the effects of unsteadiness on the boundary layer. The generation of quasisteady data is described in detail in Ref. [5]. Consider the uncorrected unsteady pressure coefficient data ($\alpha = 0°$), referenced to the static pressure at the leading edge (see Sec. II A), compared to the quasisteady data at $\phi = 90°$, $228°$, $270°$, and $314°$ in Fig. 1. The first and third phase angles correspond to $C = 0$, while the second and fourth angles correspond to the correction minimum and maximum, namely $\partial C / \partial \phi = 0$, respectively. For $C = 0$, valid comparisons between unsteady and quasisteady pressure coefficients are possible because the streamwise pressure gradient is zero. Therefore, the unsteady pressure gradient effects on the boundary layer can be inferred by comparing the unsteady and quasisteady data. In contrast, when the streamwise pressure gradient is nonzero, at $\phi = 228°$ and $314°$, the effect of the pressure gradient on the boundary layer cannot be inferred because the data are biased by the incorrect local static pressure. The bias increases linearly with $\hat{x}$ as shown in Eq. (8). Consequently, effects *of the pressure gradient on the separation bubble* cannot be separated from the effects *of the pressure gradient itself*. Thus comparisons at all phase angles presented below are based on the generalized pressure coefficient expressed in Eqs. (7) and (8), where the expression for $U(t)$ in Eq. (1) is replaced with the hot-wire measurements described in Sec. III.

Surging and quasisteady pressure coefficients are compared at $\alpha = 0°$ at selected representative phase angles in Fig. 2. High spatial resolution NACA 0018 pressure measurements by Ref. [29] show that the upstream location of almost constant pressure indicates bubble separation ($\hat{x}_{\mathrm{sep}}$), a sharp pressure rise indicates a transition ($\hat{x}_{\mathrm{tran}}$), and an abrupt decrease in slope indicates reattachment ($\hat{x}_{\mathrm{att}}$). From our relatively low spatial resolution data, $\hat{x}_{\mathrm{sep}}$ is difficult to pinpoint, but the transition location $\hat{x}_{\mathrm{tran}}$ is identifiable. In the middle of the acceleration phase ($\phi = 0°$) the quasisteady data show bubbles with a transition at $\hat{x} = 0.63$ for both the trip side and the smooth side. In contrast, for the surging case there is no clear evidence of a bubble transition on the trip side
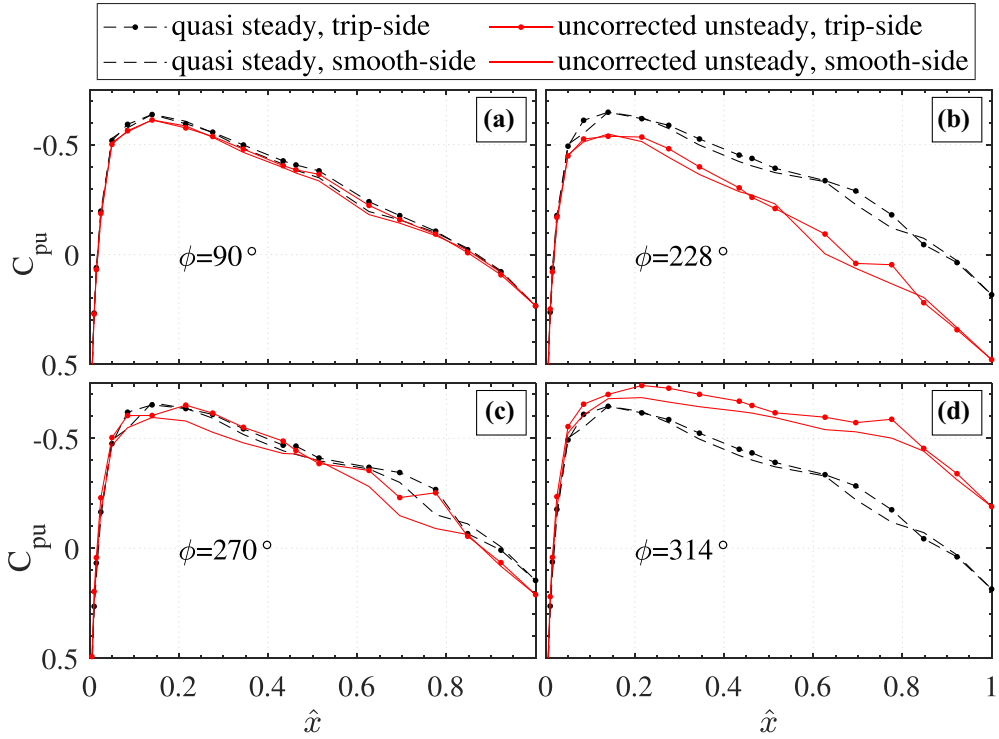
FIG. 1. Comparison of uncorrected unsteady and quasisteady pressure coefficients at phases corresponding to $C = 0$ [(a), (c)] and $\partial C/\partial \phi = 0$ [(b), (d)] for $\alpha = 0°$.
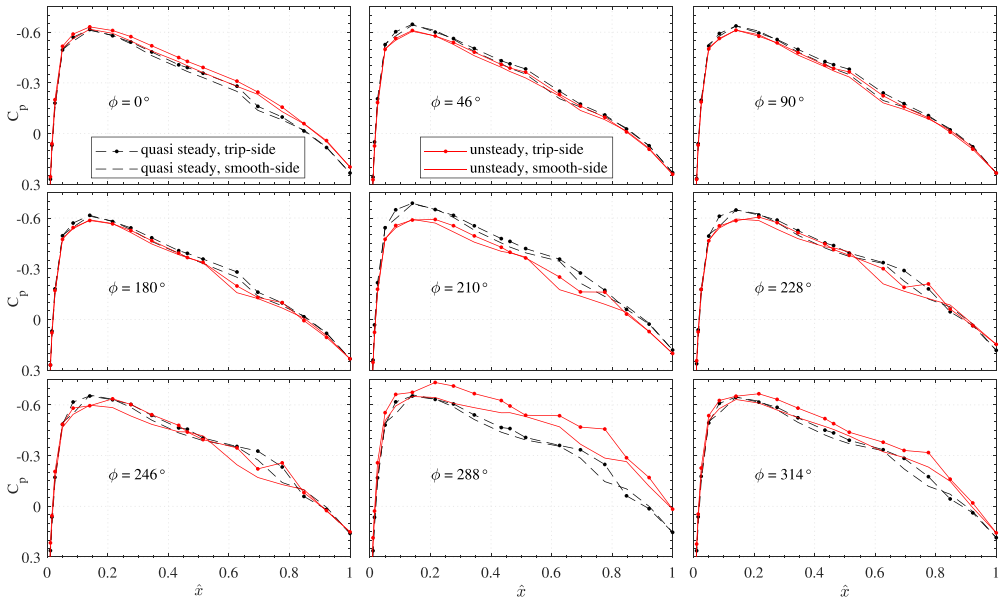

FIG. 2. Corrected unsteady and quasisteady pressure coefficients at selected representative phase angles for $\alpha = 0°$.
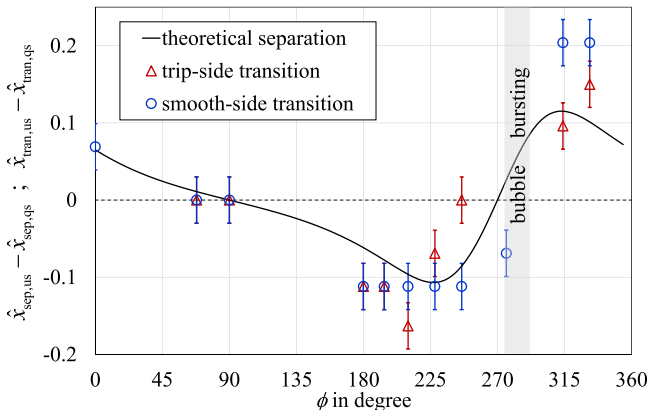
FIG. 3. Movement of the bubble separation point according to the momentum integral analysis and movement of the transition points gleaned from experimental data at $\alpha = 0°$.

and a downstream movement of a transition with a weaker pressure rise on the smooth side. As the acceleration diminishes, the bubble transition in both the surging and quasisteady cases moves gradually upstream and at the peak velocity ($\phi = 90°$), without any temporal pressure gradient, the transition locations are indistinguishable at $\hat{x} = 0.51$. This upstream movement is effected by an increase in Reynolds number and we can thus conclude that history effects are small to negligible at this phase. As the stream decelerates, both quasisteady and unsteady transitions move downstream. The movement is greater for the quasisteady case purely due to Reynolds number effects (quasi-steady data at $\phi = 0°$ and $180°$ are identical). The smaller effect in the unsteady case may be due to the upstream movement of the separation point (see Sec. II B) or due to the destabilizing effect of the deceleration, or both. During the second part of the deceleration phase, beginning at $\phi = 192°$, there is a curious pressure drop between $\hat{x} = 0.69$ and 0.78 on the trip side (Fig. 2) that increases in relative terms and is still observed at $\phi = 270°$ (not shown). Without flowfield measurements, the authors have no explanation for this, other than to speculate that the separation bubble departs dramatically from its classical form. From the angle $\phi = 276°$ to $\phi = 288°$ there is a rapid and significant drop in pressures on the aft part of the airfoil (Fig. 2). This is a clear indication that either one or both of the bubbles do not reattach, resulting in a surge-induced stall. In order to illustrate the mechanism of a surge-induced stall, and eliminate Reynolds number effects, we plot the difference, $\hat{x}_{\text{tran,us}} - \hat{x}_{\text{tran,qs}}$, together with the theoretical result, $\hat{x}_{\text{sep,us}} - \hat{x}_{\text{sep,qs}}$, from the momentum integral equation (see Sec. II B) in Fig. 3. The unsteady separation point calculation $\hat{x}_{\text{sep,us}}$ is based on the solution with both steady and unsteady pressure gradient parameters in Eq. (10), while $\hat{x}_{\text{sep,qs}}$ is based on the solution without the last term. Despite the relatively large uncertainty associated with the determination of the transition location, a qualitative correlation is evident. Theoretically, bubble separation moves rapidly downstream between $\phi = 228°$ and $314°$, but bursting is only evident for $\phi > 270°$ (see Fig. 3). Thus, in contrast to adverse spatial pressure gradients that give rise to bubble bursting and hence stall, it is in fact during the favorable pressure gradient phase of the cycle that the airfoil stalls. Namely, the rapid downstream movement of the separation point, possibly combined with stabilization due to acceleration, precipitates full separation of the bubble.

In the discussion above, we based our conclusions on the corrected pressure coefficient distributions because they provide a faithful representation of bubble separation and transition in both steady [30] and unsteady [31] flows. Nevertheless, it is clear that supplementary flowfield measurements, such as phase-resolved particle image velocimetry [29], will provide a more complete understanding of the bubble bursting mechanism. Such measurements are considered to be vital for future research of this bubble-bursting mechanism.
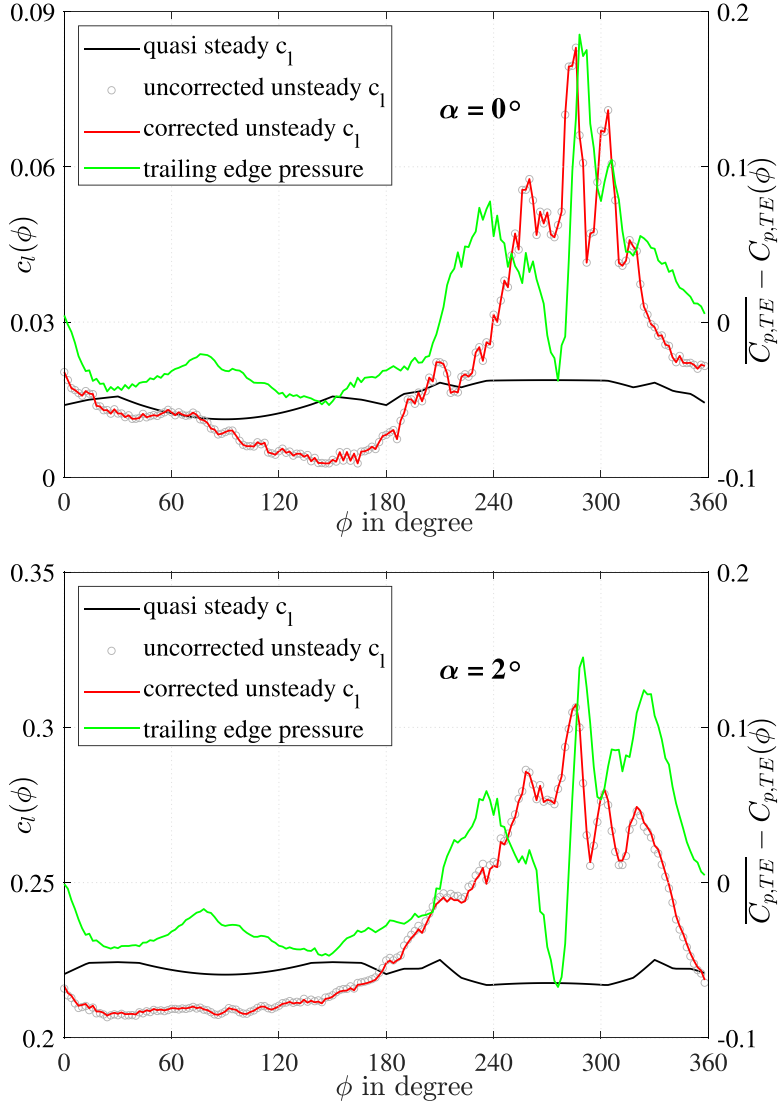
FIG. 4. Comparison of unsteady surging (corrected and uncorrected) and quasisteady lift coefficients, as well as trailing-edge pressure variations.

B. Aerodynamic coefficients

Aerodynamic coefficients were determined by integrating the pressure coefficient results, employing the method described in Ref. [32]. The corrected and uncorrected lift and pitching moment coefficients c_l and c_m are identical at $\alpha = 0°$ because both sides of the airfoil are affected equally by the correction term C in Eq. (7). At $\alpha = 2°$ they are almost identical, due to the small difference between the airfoil stagnation point location and $\hat{x} = 0$. However, the form-drag c_{dp} clearly is affected because the correction effects on both sides of the airfoil are additive. To illustrate this, both the corrected and uncorrected c_l and c_{dp} results are shown for $\alpha = 0°$ and $2°$ in Figs. 4 and 5, respectively, together with the quasisteady results and corresponding trailing-edge pressure coefficients. The lift coefficient results at both angles of attack are qualitatively similar and representative of the $0° \leqslant \alpha \leqslant 4°$ range (not shown); this indicates a similar stalling mechanism at these positive angles.
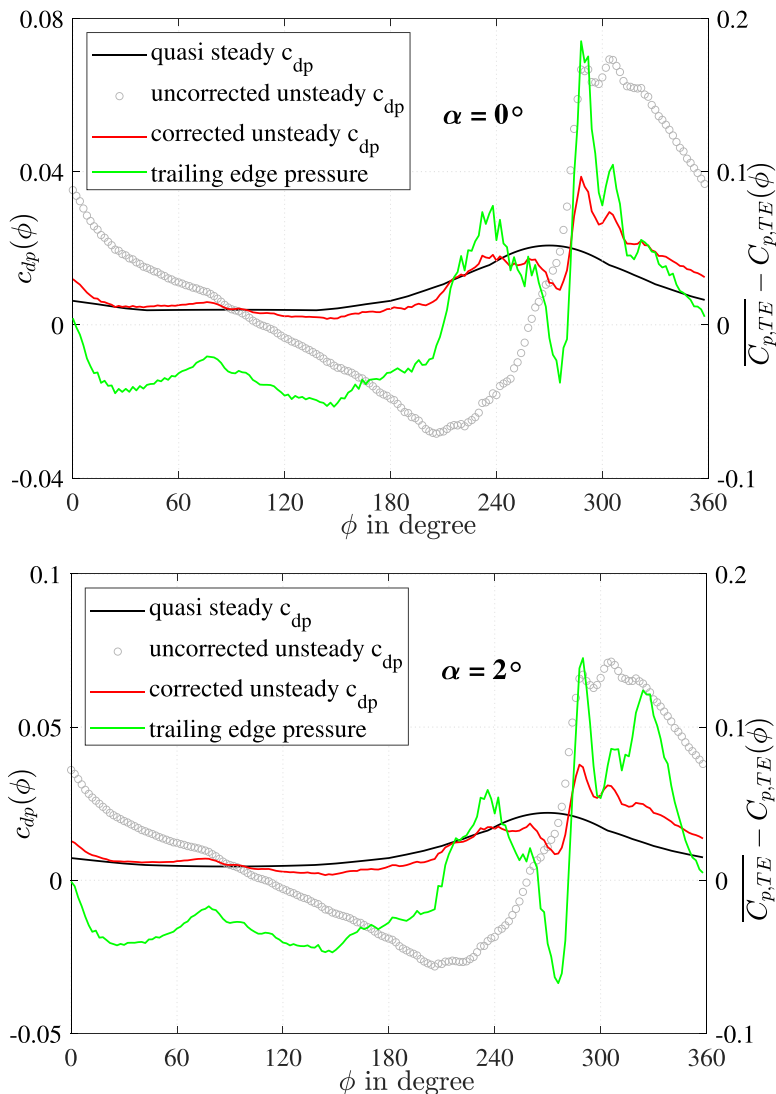
FIG. 5. Comparison of unsteady surging (corrected and uncorrected) and quasisteady form-drag coefficients, as well as trailing-edge pressure variations.

The trailing-edge pressures correlate with the integrated coefficients in the sense that local pressure minima coincide with large c_l variations ($\partial c_l/\partial \phi$). The c_l increase starting at around $\phi = 200°$ appears to be associated with the local pressure drop between $\hat{x} = 0.69$ and 0.78 discussed above, while the peaks at $\phi = 288°$ and $\phi = 306°$ are associated with bubble bursting. Similar qualitative results for $0° \leqslant \alpha \leqslant 4°$ suggest, in fact, that for $\alpha > 0°$ the smooth-side lower surface bubble bursts prior to that on the tripped side. This is because the smooth-side favorable spatial pressure gradient moves bubble separation further downstream and thus imposition of the favorable temporal pressure gradient moves the bubble too far downstream to reattach, prior to that of the trip side. Hence, the second peak, which has a smaller relative value at higher α, is associated with bursting of the trip-side bubble.

The effect of pressure coefficient correction on c_{dp} (Fig. 5) is dramatic with differences of up to 400 form-drag counts (form-drag count $= 10^4 c_{dp}$). Failure to implement the generalized pressure

coefficient results in nonphysically large negative and positive values. In fact, the uncorrected form-drag coefficient is negative over approximately half of the cycle, which incorrectly implies pressure thrust. We thus conclude that the generalized pressure coefficient is critical not only for understanding the flowfield, but also for obtaining the correct form-drag measurements. As expected, and in contrast to c_l (Fig. 4), c_{dp} and trailing-edge pressure peaks correlate directly. On the one hand, the corrected unsteady versus quasisteady comparison allows us to distinguish between purely Reynolds number effects and combined Reynolds number and unsteady effects, and on the other hand, Fig. 3 allows us to interpret the results. Specifically, the local c_{dp} reduction between $\phi = 260°$ and $270°$ is due to the upstream movement of the separation and transition points that produce higher trailing-edge pressures. This precedes the large c_{dp} peak that occurs due to lower surface bubble bursting, precipitated by the rapid downstream movement of the bubble separation point.

Differences between the cycle-averaged unsteady and quasisteady lift and moment coefficients, namely $\bar{c}_l$ and $\bar{c}_m$, are relatively small. The increases in $\bar{c}_l$ and decreases in $\bar{c}_m$ due to surging, are both $O(10^{-2})$. The phase-averaged form-drag coefficients, on the other hand, exhibit relatively large differences. For $-2° \leqslant \alpha \leqslant 4°$, $\bar{c}_{dp}$ increases by up to 75 drag counts. However, there is a crossover at $\alpha \approx -2.5°$, where surging reduces $\bar{c}_{dp}$ by 40 and 50 counts at $\alpha = -3°$ and $-4°$, respectively.

The bubble-bursting mechanism described above was not observed in previous investigations, for two main reasons. First, virtually all of the other experiments were performed at relatively high poststall angles [4,5,7,8,10], and hence the drag correction is an order of magnitude greater than the nominal values. Second, most experiments are performed at Reynolds numbers less than or equal to 10^5, where the bubble transition occurs too far downstream for the boundary layer to reattach [33].

V. CONCLUSIONS

The effect of unsteady, periodic, surging flows on airfoil separation bubble behavior at low angles of attack was evaluated experimentally and theoretically. A generalized pressure coefficient was defined and the effects of surging were determined by comparing unsteady and quasisteady pressure coefficients. Furthermore, a quasisteady momentum integral boundary layer analysis was employed to predict changes in the bubble separation point. The analysis and data pointed to a stabilizing effect during the latter part of the acceleration that produced downstream movement of the bubble. Deceleration, on the other hand, produced upstream movement of the bubble, when Reynolds number effects were accounted for. Counterintuitively, a surge-induced stall occurred during the early part of the acceleration phase. This was precipitated by the rapid downstream movement of bubble separation, shown theoretically and experimentally, accompanied by large lift and form-drag coefficient oscillations. Lift and form-drag coefficient behaviors were qualitatively similar for $0° \leqslant \alpha \leqslant 4°$, which suggests that the smooth, lower surface, bubble bursts prior to that on the tripped upper surface. In future research, detailed high spatial resolution pressure and flowfield measurements should be made to precisely quantify the complex flowfield produced by temporal pressure gradients.

[1] M. Brendel and T. J. Mueller, Boundary layer measurements on an airfoil at a low Reynolds number in an oscillating freestream, AIAA J. **26**, 257 (1988).

[2] J. P. J. Retelle, Unsteady boundary layer flow reversal in a longitudinally oscillating flow, Ph.D. thesis, University of Colorado, 1978.

[3] W. Zhu, M. H. McCrink, J. P. Bons, and J. W. Gregory, The unsteady Kutta condition on an airfoil in a surging flow, J. Fluid Mech. **893**, R2 (2020).

[4] R. Dunne and B. J. McKeon, Dynamic stall on a pitching and surging airfoil, Exp. Fluids **56**, 157 (2015).

[5] H. F. Müller-Vahl, C. Strangfeld, C. N. Nayeri, C. O. Paschereit, and D. Greenblatt, Dynamic stall under combined pitching and surging, AIAA J. **58**, 5134 (2020).

[6] D. Simms, S. Schreck, M. Hand, and L. J. Fingersh, NREL unsteady aerodynamics experiment in the NASA-Ames wind tunnel: A comparison of predictions to measurements, Technical Report No. NREL/TP-500-29494, National Renewable Energy Laboratory, Golden, Colorado, 2001.

[7] K. Granlund, B. Monnier, M. Ol, and D. Williams, Airfoil longitudinal gust response in separated vs. attached flows, Phys. Fluids **26**, 027103 (2014).

[8] J. Choi, T. Colonius, and D. R. Williams, Surging and plunging oscillations of an airfoil at low Reynolds number, J. Fluid Mech. **763**, 237 (2015).

[9] A. Medina, M. V. Ol, D. Greenblatt, H. Müller-Vahl, and C. Strangfeld, High-amplitude surge of a pitching airfoil: Complementary wind- and water-tunnel measurements, AIAA J. **56**, 1703 (2018).

[10] P. B. Kirk and A. R. Jones, Vortex formation on surging aerofoils with application to reverse flow modelling, J. Fluid Mech. **859**, 59 (2019).

[11] C. Strangfeld, H. Müller-Vahl, C. N. Nayeri, C. O. Paschereit, and D. Greenblatt, Airfoil in a high amplitude oscillating stream, J. Fluid Mech. **793**, 79 (2016).

[12] J. M. Greenberg, Airfoil in Sinusoidal Motion in a Pulsating Stream, Technical Report No. NACA TN1326, National Advisory Committee for Aeronautics, Hampton, Virginia, 1947.

[13] R. Isaacs, Airfoil theory for flows of variable velocity, J. Aeronaut. Sci. **12**, 113 (1945).

[14] B. G. van der Wall and J. G. Leishman, On the influence of time-varying flow velocity on unsteady aerodynamics, J. Am. Helicopter Soc. **39**, 25 (1994).

[15] M. Gaster, The structure and behaviour of laminar separation bubbles, Reports and Memoranda No. 3595 (Aeronautical Research Council, London, 1967).

[16] O. Marxen and U. Rist, Mean flow deformation in a laminar separation bubble: separation and stability characteristics, J. Fluid Mech. **660**, 37 (2010).

[17] O. Marxen, M. Lang, U. Rist, and S. Wagner, A combined experimental/numerical study of unsteady phenomena in a laminar separation bubble, Flow, Turbul. Combust. **71**, 133 (2003).

[18] S. Pröbsting and S. Yarusevych, Laminar separation bubble development on an airfoil emitting tonal noise, J. Fluid Mech. **780**, 167 (2015).

[19] S. S. Diwan and O. Ramesh, On the origin of the inflectional instability of a laminar separation bubble, J. Fluid Mech. **629**, 263 (2009).

[20] S. S. Diwan, S. Chetan, and O. Ramesh, On the bursting criterion for laminar separation bubbles, in *IUTAM Symposium on Laminar-Turbulent Transition* (Springer, Berlin, 2006), pp. 401–407.

[21] M. M. O'Meara and T. J. Mueller, Laminar separation bubble characteristics on an airfoil at low Reynolds numbers, AIAA J. **25**, 1033 (1987).

[22] P. R. Spalart and M. K. Strelets, Mechanisms of transition and heat transfer in a separation bubble, J. Fluid Mech. **403**, 329 (2000).

[23] E. Malkiel and R. Mayle, Transition in a separation bubble, J. Turbomach. **118**, 752 (1996).

[24] R. Wickens, Wind tunnel investigation of dynamic stall of an NACA 0018 airfoil oscillating in pitch, Aeronautical Note NAE-AN-27, NRC No. 24262 (National Aeronautical Establishment, Ottawa, Canada, 1985).

[25] H. Schlichting and K. Gersten, *Boundary Layer Theory*, 9th ed. (Springer, Berlin, 2017).

[26] R. G. Docken, Jr., Gust response prediction of an airfoil using a modified von Karman–Pohlhausen technique, Master's thesis, Air Force Institute of Technology, Air University, Ohio, 1982.

[27] M. Drela, XFOIL: An analysis and design system for low Reynolds number airfoils, in *Low Reynolds Number Aerodynamics* (Springer, Berlin, 1989), pp. 1–12.

[28] D. Greenblatt, Unsteady low-speed wind tunnels, AIAA J. **54**, 1817 (2016).

[29] J. W. Kurelek, A. R. Lambert, and S. Yarusevych, Coherent structures in the transition process of a laminar separation bubble, AIAA J. **54**, 2295 (2016).

[30] R. Gerakopulos and S. Yaruseyvich, Novel time-resolved pressure measurements on an airfoil at a low Reynolds number, AIAA J. **50**, 1189 (2012).

[31] H. Müller-Vahl, C. Strangfeld, C. N. Nayeri, C. O. Paschereit, and D. Greenblatt, Control of thick airfoil, deep dynamic stall using steady blowing, AIAA J. **53**, 277 (2015).

[32] J. D. Anderson, *Fundamentals of Aerodynamics* (McGraw-Hill, Singapore, 2011).

[33] B. H. Carmichael, Low reynolds number airfoil survey, Vol. 1, Technical Report No. NASA-CR-165803-VOL-1 (Low Energy Transportation Systems, Capistrano Beach, CA, 1981).